Femtosecond response in rare gas matrices doped with NO impurities: A stochastic approach

G. Rojas-Lorenzo,¹ A. S. Sanz,² J. Rubayo-Soneira,³ and S. Miret-Artés²

¹Instituto Superior de Tecnologías y Ciencias Aplicadas,

Ave. Salvador Allende, esq. Luaces, 10400 - La Habana, Cuba

²Instituto de Física Fundamental, Consejo Superior de

Investigaciones Científicas, Serrano 123, 28006 Madrid, Spain

³Instituto Superior de Tecnologías y Ciencias Aplicadas,

Ave. Salvador Allende, esq. Luaces, 10400 - La Habana, Cuba

Abstract

The femtosecond response of NO-doped rare gas matrices is studied within a stochastic Langevin theoretical framework. As is shown, a simple damped harmonic oscillator model can describe properly the absorption and emission line shapes associated with the NO $(A^2\Sigma^+ \longleftrightarrow X^2\Pi)$ electronic transitions inside these media as well as the matrix first-solvation shell response in a process with two timescales, finding a fairly good agreement with available experimental data. This approach thus constitutes an alternative and complementary way to analyze the structural relaxation dynamics of systems in liquids and solids, leading to a better understanding of the underlying physics.

Many molecular systems undergo local structural changes when they are photoexcited to electronic states with strong electron-phonon couplings. These structural changes may lead to an important reorganization of the surrounding medium [1, 2]. In this regard, due to their simple structural and well-known physical and thermodynamical properties, pure and doped rare gas matrices constitute an ideal benchmark to analyze and understand the fundamental mechanisms of configurational rearrangements in more complex molecular systems [1, 3, 4, 5]. Among them, NO-doped rare gas matrices result of particular interest due to the many conventional (steady-state) [6, 7, 8, 9, 10, 11] and femtosecond pump-probe [11, 12, 13, 14, 15, 16] spectroscopy experimental studies available for these systems, which reveal the medium dynamical response when the NO molecule is photoexcited to one of its lowest Rydberg states.

From previous studies in the literature [6, 7, 12, 14], the dynamics associated with the NO electronic transition between the ground state (X) and one of its lowest Rydberg excited states (e.g., A) can be described as a four-step process [7, 9, 10] within the configuration coordinate model in the harmonic approximation (CCM-HA), which allows us to relate experimental spectroscopic information to the potential energy surfaces of the different electronic states of the impurity. The four-step process is essentially as follows. In a first step, the absorption of a photon excites the only unpaired electron of the NO molecule to a Rydberg state. This provokes an overlapping between the NO Rydberg orbital and the matrix shells constituted by the neighboring rare gas (Rg) atoms due to the larger effective size of the new NO excited state with respect to its ground state. As a consequence, the atoms of the first solvation shell undergo a strong repulsion, which displaces them from their equilibrium positions and, therefore, leads to an increase of the NO-matrix bond lengths. Because the process is energetically unfavorable, in a second step, the lattice relaxes around the excited impurity, with the Rg-atoms reaching a new equilibrium position. During this process, most of the energy in excess is dissipated through the matrix, but a small fraction is invested into an expansion of the surroundings beyond the first solvation shell. This latter amount of energy is going to contribute substantially to the restoring force in the next step. This basic mechanism consisting of an oscillating radial expansion/compression of the cage around the NO molecule, from one equilibrium cage radius to another one, is known as the electronic bubble formation [1, 2, 3, 4, 7], and is also operative in rare gas liquids and clusters [1, 2, 17, 18, 19, 20]. For instance, molecular dynamics simulations of this bubble formation have been carried out [21, 22, 23] to interpret the absorption and fluorescence spectra of Xe-dopped Ar_n clusters upon photoexcitation of the Xe dopant to low-n Rydberg states [17, 18, 19, 20]. In the case of photoexcited impurities trapped in rare gases and van der Waals solids, an extensive literature can also be found [1, 3, 4, 6, 7, 8, 12, 13, 24, 25]. In a third step, Rydberg fluorescence with the emission of a photon may occur, which (fourth step) brings the system back to its initial ground state configuration by relaxation, leading to the equilibrium cage radius associated with the NO ground state.

As infers from the above described absorption/emission process, the first and third steps are related to energetic aspects of the transition (steady-state spectroscopy), while the second and fourth steps are associated with the solvent relaxation dynamics (femtosecond pump-probe spectroscopy). In general, all rare gas matrices respond to photoexcitation by undergoing an ultrafast expansion of the first solvation shell during the first 100-200 fs (something similar also happens in the case of the emission process), where almost all the solute-solvent interaction energy becomes kinetic. During this expansion, the cage radius reaches a maximum above $r_{eq}^{(A)}$, the equilibrium cage radius for the NO molecule in its Rydberg excited state, and then gets back below it (but always above $r_{eq}^{(X)}$, the equilibrium cage radius for the NO molecule in its ground state). The time at which the cage radius reaches this first minimum is the so-called first recurrence time τ [11, 14, 15, 16]. Due to the energy relaxation process, for any time $t > \tau$, the cage radius fluctuates with decreasing amplitude around $r_{eq}^{(A)}$, which is finally reached asymptotically (like a damped motion).

The ultrafast lattice structural dynamics mediated by NO excitation has been studied in the last years by means of classical molecular dynamics (CMD) [26, 27, 28, 29], obtaining a reasonable agreement with the experimental data. Apart from numerical issues (e.g., introduction of periodic boundary conditions, cutoff radii or smoothing functions to avoid 'border effects'), an important source for deviations between CMD-based simulations and experiment [9, 10] is the unavailability of accurate interatomic potential surfaces describing the NO(A)-Rg interaction, where Rg = Ne, R, R or R. Therefore, the standard procedure to obtain the potential surface is by considering pairwise potential models and then carrying out simulations where the parameters defining such models are varied until an optimal fit to the experimental data is found. Non-equilibrium and dissipative properties involved in this kind of processes (e.g., dissipation, relaxation or friction) can also be studied by means of CMD. Nevertheless, besides CMD simulations, these properties can also be extracted

alternatively by means of a stochastic approach, which renders a complementary view of the dynamics underlying the corresponding experimental findings.

Here, we propose a fully stochastic classical Langevin model (CLM) to tackle the problem of the analysis and interpretation of the lattice relaxation dynamics of NO-doped rare gas matrices. More specifically, making use of the CCM-HA [7, 9, 10], where the pairwise impurity-lattice and lattice-lattice interactions are substituted by a global cage harmonic potential, the structural relaxation of the first solvation shell of the solid matrix is described in terms of a simple damped harmonic oscillator (DHO) model, where the energy transfer to/from the remaining shells of the rare gas matrix (heat bath) is accounted for by a damping rate [30, 31]. In this way, the DHO-CLM used here avoids the problem of considering explicitly particular many-body potential energy surfaces, this resulting in a gain of analytical handiness and, therefore, of physical insight. Moreover, it also entails a considerable save of computational time, something very important when one is interested in the global understanding and fitting procedure of the experimental data rather than in a detailed dynamics accounting for them. In this regard, CLM-based approaches have been successfully used to study surface diffusion [32, 33, 34, 35, 36]. It is worth stressing that, though the Langevin equation employed in CLMs is seemingly phenomenological, it can be formally derived from the so-called Caldeira-Leggett Hamiltonian [37, 38, 39, 40, 41, 42, 43], very well known in the theory of open quantum systems [30, 31]. The Caldeira-Leggett Hamiltonian, introduced in the dynamics of open classical/quantum systems in 1983, shows that the effects of the detailed dynamics of a given bath or thermal reservoir (solid, liquid, etc.) acting on a system can be replaced by an infinite sum of harmonic oscillators. The damping acting over the system can be expressed, in general, as a time-dependent function involving the corresponding harmonic frequencies and the system-bath coupling constants. When the damping function becomes Ohmic (i.e., it is described by a constant spectral function of the frequency), the generalized Langevin equation (arising from the Caldeira-Leggett Hamiltonian) describing the system evolution reduces to a standard Langevin equation.

In the problem of NO-doped rare gas matrices, the electron-phonon coupling during the electron excitation has been estimated from the experiment [7] and is directly related to the displacements of the equilibrium configuration coordinate in the ground and excited states. On the other hand, the lattice relaxation (first solvation shell) can be described by a new damping rate which gives us an idea of the energy loss to the Rg-atom matrix acting

as a heat bath via a sort of *effective* phonon-phonon coupling after excitation within the electronic bubble model. The dynamics of the cage radius involving the first solvation shell is coupled to the remaining solvation shells displaying a damped harmonic oscillation. As will be shown below, this damping rate introduces a new timescale.

Thus, the NO absorption/emission spectrum is related to the response of the matrix first solvation shell (i.e., the shell of first nearest neighbors around the impurity). In order to describe the dynamical evolution of the first solvation shell, the CCM-HA is commonly used in the literature [7, 9, 10], with the configuration coordinate being the *matrix cage radius*, r. Within this model, r represents the mean distance between the NO impurity and each one of the atoms of the first solvation shell, and an effective harmonic potential (per mass unit),

$$U(r) = \frac{1}{2}\omega_0^2(r - r_{eq})^2,\tag{1}$$

stands for the impurity-matrix interaction. In (1), ω_0 is the effective harmonic frequency [7, 9, 10] and r_{eq} is the equilibrium cage radius of the first solvation shell [27, 28, 29]; $r_{eq}^{(A)}$ and $r_{eq}^{(X)}$ will denote the equilibrium cage radii after absorption and emission, respectively. Estimates of the harmonic frequency and the cage radius increment, $\Delta \equiv r_{eq}^{(A)} - r_{eq}^{(X)}$, have been obtained in the literature for different matrices from a direct analysis of experimental spectroscopic data by using either the method of moments [7] or the semiclassical projection method [9, 10]. The so-called Huang-Rhys factors [7] suggest a decreasing electron-phonon coupling with the rare gas mass forming the solid matrix. This can be understood by taking into account the fact that, as the Rg atom mass increases, the characteristic NO-Rg bond lengths, and also the Rg-Rg ones, become larger and, therefore, the NO Rydberg orbital can be better accommodated within the space inside the first solvation shell. The values of the effective harmonic frequency in the excited state, $\omega_0^{(A)}$, as well as the cage radius increment found for NO-Rg matrices, with Rg = Ne, Ar, Kr and Xe, are given in Table I. As can be noticed, while Δ decreases monotonically as the NO-Rg and Rg-Rg bond length increase for ω_0 , the variation with the mass follows the opposite trend. Notice that an increase of ω_0 with the mass results counterintuitive, for one would be tempted to think that heavier particles will oscillate slower than lighter ones. As will be shown, in our model the ω_0 frequencies, as well as the corresponding recurrence times, will be modified due to the presence of the damping rate.

After assuming the CCM-HA, the effects of the energy transfer process between the first

TABLE I: Effective harmonic frequencies associated with the NO in the ground $(\omega_0^{(X)})$ and the Rydberg excited $(\omega_0^{(A)})$ states, and increment of the NO-Rg cage radius (Δ) for Rg = Ne, Ar, Kr and Xe, within the configuration coordinate model in the harmonic approximation. For Ne, Ar and Xe, the value of these magnitudes have been taken from Ref. [10], while for Kr they are from Ref. [7].

	Ne	Ar	Kr	Xe
$\omega_0^{(X)} \text{ (ps}^{-1})$	1.26	1.23	1.35	1.53
$\omega_0^{(A)} \; (\mathrm{ps}^{-1})$	1.74	1.41	1.45	1.59
$\Delta \ (ext{Å})$	0.59	0.41	0.18	0.14

solvation shell and the remaining shells from the solid matrix can be described in terms of the cage radius by means of the Langevin equation associated with a DHO, as

$$\ddot{r}(t) = -\gamma \, \dot{r}(t) + F[r(t)] + \xi(t). \tag{2}$$

In this equation, $F = -\nabla U$ is the deterministic force (per mass unit) acting over the first solvation shell. The fluctuating force, $\xi(t)$, is described by a Gaussian white noise, thus satisfying $\langle \xi(t) \rangle = 0$ and $\langle \xi(t)\xi(t') \rangle = 2\mu\gamma k_B T\delta(t-t')$, where μ is the effective mass associated with the first solvation shell, i.e., its value is 12 times the Rg-atom mass [7, 9, 10], T is the temperature and k_B the Boltzmann constant. Furthermore, γ is a constant damping rate related to the fluctuating force $\xi(t)$ through the fluctuation-dissipation theorem [30, 31]. As can be noticed, Eq. (2) is a standard Langevin equation, which is used instead of its generalized version because the relaxation time at which the system (the cage radius) approaches equilibrium with the heat bath is much longer than the correlation time of the bath fluctuations (Markovian approximation). Phenomenological values of γ have been used in the literature in stochastic Langevin theoretical treatments to describe solute-solvent energy exchange in liquids and solids [44, 45, 46, 47], though it is more commonly related to liquids and gases.

In our simulations, 10,000 stochastic trajectories have been run for each electronic state up to 5 ps, considering time steps of 1 fs. Initial conditions are assigned like in the corresponding CMD simulations [26, 27, 28, 29]. The initial positions are randomly generated according to a uniform distribution centered around $r_{eq}^{(X)}$ or $r_{eq}^{(A)}$, depending on whether emission or

TABLE II: Optimal values of γ obtained from the DHO-CLM. This damping rate governs the relaxation dynamics in the ground state after emission (γ_X) or the excited state after absorption (γ_A) .

	Ne	Ar	m Kr	Xe
$\gamma_X \text{ (ps}^{-1})$	0.51	0.57	0.67	1.15
$\gamma_A \; (\mathrm{ps}^{-1})$	0.51	0.61	1.05	1.55

absorption are being studied, respectively. Regarding the choice of the initial velocities, they follow a standard Boltzman distribution at a temperature T. The experiments are carried out at T=4 K, where the nuclear dynamics of the matrix atoms is dominated by the zero-point motion. Hence, in order to account for this quantum effect properly in CMD simulations, a higher effective temperature depending on the Debye frequency of the solid has to be considered [48] (e.g., for a solid Ar matrix, the effective temperature corresponding to T=4 K is about 49 K). Thus, the initial velocities have to be re-scaled accordingly (i.e., taking into account this effective temperature) before starting the simulation, which we have carried out by using the velocity-Verlet algorithm [49] to propagate in time the stochastic trajectories. Then, the absorption and emission bands are calculated by constructing histograms with the energy differences between the initial (ground state for absorption, excited state for emission) and the final state (excited state for absorption, ground state for emission). In particular, we have considered the electronic transition between the NO ground state and its first lowest Rydberg state, i.e., $A^2\Sigma^+\longleftrightarrow X^2\Pi$. The medium response to the electronic transition is induced by an instantaneous switching from the ground state potential to the excited one (making use of the Franck-Condon principle). Now, in order to reproduce the experimental bandwidths, γ is chosen as the only fitting parameter (remember that in the homologous CMD simulations, the fitting parameters usually appear in the potential energy surface models considered), which is varied until the band widths are fairly reproduced. The optimal γ values obtained from the DHO-CLM are given in Table II. These values deviate less than 10% from the rates obtained through CMD after computing the approximated time exponential decay of the total energy autocorrelation function for the impurity,

$$C_E(t) = \langle E(t)E(t-t_0)\rangle - \langle E^2(t)\rangle. \tag{3}$$

From this expression one can extract the rate of energy transfer between the first solvation shell and the surrounding bath during the corresponding relaxation process and, therefore, of the cage radius damping towards its equilibrium value. Fortunately, the band widths are not very sensitive to the γ rates allowing us a certain degree of flexibility in the fitting procedure. As can be seen, γ increases from Ne to Xe matrices and is always larger in the excited than in the ground state. Physically, this indicates an important energy loss between the first solvation shell and the medium or heat bath via an effective phonon-phonon coupling, which increases with the mass of the species constituting the solid matrix and, therefore, its rigidity. Moreover, this energy loss is also larger when the impurity is photoexcited. In the experiment and also in CMD simulations, a rapid relaxation of the photoexcited NO molecules to the medium is observed [26, 27, 28, 29] for Ar, Kr and Xe matrices, while for Ne matrices the effect is slower and "collective" (see below). Finally, as Eq. (2) describes the dynamics of the first solvation shell, γ^{-1} will also provide a timescale for the solvent relaxation dynamics, which ranges from \sim 650 fs for NO(A) in Xe to \sim 2,000 fs in Ne.

In Fig. 1, absorption (right/blue) and emission (left/red) bands obtained from the DHO-CLM simulations are plotted for matrices constituted by different Rg-atoms and compared with the corresponding experimental data (dots). These steady-state absorption and emission bands represent the initial and final stages of the photoinduced structural rearrangement process around the excited NO molecules. To compare with the effects produced by the presence of the matrix, the green horizontal dashed line around 5.5 eV indicates the position of the NO absorption/emission electronic transition in the gas phase. As can be noticed, the line shapes of the bands and their Stokes shifts are in good agreement with the experimental data, the main differences being lower than 2% in all cases. Larger numerical discrepancies can be found, however, in the CMD simulations [26, 27]. For example, for Ar matrices, the DHO-CLM reproduces quite accurately the experimental value of the Stokes shift, 0.570 eV [7], while the CMD calculations provide a shift of 0.700 eV [26, 27]. In the case of Ne, the shift obtained from CMD is not so good in comparison with the experiment and depends strongly on the parameters of the pairwise potentials considered. On the other hand, although for Kr and Xe matrices both the DHO-CLM and CMD [29] simulations reproduce fairly well the experimental value of the Stokes shift [7], the corresponding line shapes have not been calculated from the latter.

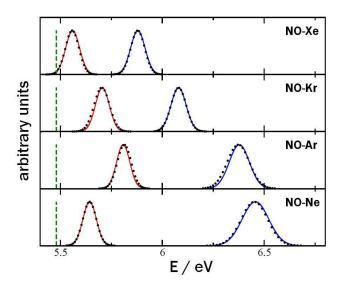


FIG. 1: (Color online.) Absorption (right/blue) and emission (left/red) line shapes associated with the NO ($A^2\Sigma^+ \leftrightarrow X^2\Pi$) electronic transition in rare gas solids. In all cases, experimental data are represented by dots, while the line shapes obtained with the DHO-CLM are denoted by solid lines. The green horizontal dashed line around 5.5 eV denotes the position of the same absorption/emission process, but for the NO molecule in gas phase.

The time evolution of the cage radius after the absorption is plotted in Fig. 2(a), where the cage radius is expressed in terms of its effective increase, $r' = r - r_{eq}^{(X)}$. In this way, at t = 0, r' = 0 means that the cage radius starts at $r = r_{eq}^{(X)}$; on the contrary, asymptotically, in the limit $t \to \infty$, r' will approach the cage radius increment Δ , since the cage radius approaches the equilibrium value, $r_{eq}^{(A)}$. Physically, this curve describes a process with two different timescales. The first part of the process consists of the initial cage radius expansion (from t = 0 to the first maximum) and indicates the matrix response after a photon is absorbed by NO and its unpaired electron is promoted to the Rydberg state, thus increasing the effective size of the impurity (and so the size of the bubble). As seen in Fig. 2(a), this expansion (solid line) is relatively fast and mimicking the CMD results (blue dotted line) for about the first 150 fs in all cases. In particular, the maximum expansion velocity (slope) reached by the first solvation shell is 471 m/s (139 fs) for Ne-matrices, 308 m/s (171 fs) for Ar-matrices, 167 m/s (163 fs) for Kr-matrices, and 114 m/s (141 fs) for Xe-matrices (between brackets, the time at which this velocity is reached), which are similar to those obtained from CMD [14]. However, because the electron-phonon coupling decreases with the Rg-atom mass, as

derived from the method of moments in Ref. [7], not only a smaller increase of the cage radius from Ne to Xe matrices is noticeable, but also in the initial slope of its evolution, as seen in Fig. 2(b). The second part of the process describes the relaxation of the cage radius to its equilibrium value after the initial boosting led by the (ultrafast) expansion of the NO orbital. This is the stage that follows the first maximum in the curves displayed in Fig. 2(a). As can be noticed, the damping of the oscillations around the corresponding equilibrium cage radius increases from Ne to Xe matrices, this being indicated by an also increasing value of γ (which we have obtained from the fitting to the experimental spectroscopic measures, as indicated above). According to the DHO model, the corresponding oscillations displayed in Fig. 2 and their envelopes follow an expression of the type $e^{-\gamma t/2} \cos(\bar{\omega}t + \delta)$, where the renormalized harmonic frequencies are given [30] by

$$\bar{\omega} = \sqrt{\omega_0^2 - \frac{\gamma^2}{4}} \tag{4}$$

and the phase shift by $\delta = \tan^{-1}(\gamma/2\bar{\omega})$. From Ne to Xe matrices, these renormalized frequencies are 1.72, 1.38, 1.35, and 1.39 ps⁻¹, respectively. These values follow the same tendency observed in the experiment [7] by means of an analysis carried out by the method of moments (see Table I). In principle, a larger damping implies a lower oscillation, which stresses with the fact that the Rg-atom mass increases. In other words, intuitively, one should expect that the heavier the Rg-atom mass, the slower the oscillation and, therefore, the larger the recurrence times (which are discussed below). In order to understand this counterintuitive behavior, remember that bond lengths increase with the Rg-atom mass and, therefore, one could expect a matrix response more typical of rigid solids for larger Rg atoms, and more "floppy", i.e., involving more neighboring shells, for smaller Rg atoms. If so, as happens with sound waves, the transmission of energy through the material is more effective (faster) for solids than for liquid which, within the context of our model, means greater energy losses to the first-neighbors shells as the Rg-atom mass increases.

As shown in Fig. 2(a), for Ne matrices the DHO-CLM renders a value for the first recurrence time of $\tau_{\rm DHO-CLM} \approx 564$ fs, which does not agree with the experimental value $\tau_{\rm exp} \approx 1.1\text{-}1.4$ ps [15, 16]. In the case of CMD, in order to obtain a good estimate of this time, an artificially shortened Born-Mayer potential model was considered, which provides $\tau_{\rm CMD} \approx 1.3$ ps [15, 28]. To understand this discrepancy, as mentioned above, note that the NO(X)-Ne and Ne-Ne bond lengths are smaller than the NO(A)-Ne one, which covers

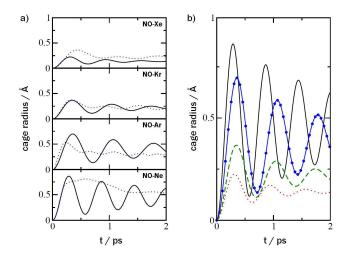


FIG. 2: (Color online.) Cage radius dynamics. a) Blue dotted lines have been obtained from CMD simulations [27, 28, 29], while black solid lines represent the results from the DHO-CLM. b) Comparison of the four cases considered in part (a): Ne-matrix (black solid line), Ar-matrix (blue solid line with circles), Kr-matrix (green dashed line) and Xe-matrix (red dotted line).

about four solvation shells [15, 28]. Thus, although the initial expansion of the cage radius is well described by the DHO-CLM because it is only affected by the first solvation shell, immediately after such an expansion the size of the excited NO wave function overlaps the matrix atoms of upper shells, which are not considered in the DHO-CLM. The contribution of these upper shells would lead to observe the first recurrence at longer times due to a slower relaxation (i.e., a "floppy"-like matrix behavior under a local structural perturbation). The recurrence time, therefore, would not be ruled by one shell but by four shells at a time, as shown through CMD [15, 28]. A simple way to deal with this effect consists of including an anharmonic contribution in the effective potential acting over the solvation shell in the involved excited state. This procedure improves the value of the recurrence time to be $\tau_{\mathrm{DHO-CLM}} \approx 1.09$ ps and leaves unchanged the corresponding line shapes. Obviously, this is the simplest and fastest way of considering the inclusion of more external shells. Other more elaborated schemes can be envisaged such as, for example, using a four-variable model with four coupled Langevin equations, each one describing the evolution of the radius associated with each shell. In the case of Ar matrices, we find a recurrence time greater than in the corresponding CMD calculation [see Fig. 2(a)], $\tau_{\rm CMD} \approx 500$ fs [14] versus $\tau_{\rm DHO-CLM} \approx 711$ fs, in better agreement with the experimental value $\tau_{\rm exp} \approx 600$ -800 fs [14, 16]. Contrary to the case of Ne, here the NO(A)-Ar bond length is such that the expansion of the NO wave function up to $t \sim \tau$ is going to affect essentially the first solvation shell and, therefore, the dynamics will be well reproduced. Note that, as μ increases (from Ne to Xe), the amplitude of the expansion curve of the cage radius decreases as well as the expansion velocity of the solvent shell. However, the first recurrence time is not an increasing monotomic function of the mass, as observes in Fig. 2(b). With respect to Kr matrices, we have found an acceptable similarity in the response between DHO-CLM and CMD [note in Fig. 2(a) that $\tau_{\text{DHO-CLM}} \approx \tau_{\text{CMD}}$]. For Xe matrices, both simulations provide a similar behavior pattern qualitatively (regarding the amplitude of the oscillations) though some quantitative discrepancies can be found. To our knowledge, there are no reported femtosecond experiments for the bubble dynamics in Kr and Xe matrices and, therefore, the corresponding curves (as also happens with those obtained from CMD) have to be considered as predictive.

Summarizing, we have shown that the experimental absorption/emission bands associated with the $A^2\Sigma^+ \leftrightarrow X^2\Pi$ electronic transition of NO in rare gas matrices can be fairly well reproduced by means of a simple damped harmonic oscillator model, which describes the dynamics of the first solvation shell (i.e., the response of the matrix to the NO excitation) in a process with two different timescales. The first part of the process (fast expansion of the first solvation shell) is directly related to the electron-phonon coupling which has measured in the experiment. In the second part of the process, the introduction of a new damping rate via an effective phonon-phonon coupling after excitation in order to describe the lattice relaxation allows us to obtain very reliable band structures by only using data from spectroscopic measurements and a single fitting parameter (γ) . As shown, the expansion dynamics of the cage radius is well described for about the first 200 fs as well as the first recurrence time. Our DHO-CLM should improve with the mass of the matrix atoms. Note that the calculation of τ from the model presented here marks the time at which a well-defined first recurrence takes place. Nonetheless, the fact that only the first solvation shell is involved in the dynamics described restricts the applicability of the model when 'collective' shell behaviors are present, as in the case of Ne matrices. In such cases, it has been shown that the addition of anharmonic contributions to the effective harmonic potential used, which would account for the eventual distortions undergone by the first solvation shell, render better recurrence times in comparison with the experimental ones. For Ar matrices, $\tau_{\rm DHO-CLM}$ agrees fairly well with the experimental value without any need to consider anharmonicities. The oscillations of the cage radius as well as the recurrence times are easily explained within the DHO model through a renormalization of the harmonic frequencies due to the presence of the damping rate. This information could be therefore used to design new femtosecond pump-probe experiments. The fact that all of these features are reasonably well reproduced by simple, stochastic Langevin simulations opens up a new theoretical way to explore, describe and understand the physics underlying rearrangement processes in solids, stressing the insightful value of the model.

We would like to acknowledge fruitful discussions with Prof. Majed Chergui. We also highly appreciate the very constructive and positive comments made by one of the referees. This work has been supported by the Ministerio de Ciencia e Innovación (Spain) under Projects FIS2007-62006 and SB2006-0011. A.S. Sanz acknowledges the Consejo Superior de Investigaciones Científicas for a JAE-Doc Contract.

^[1] N. Schwentner, E.E. Koch, J. Jortner, Electronic Excitation in Condensed Rare Gas Solids, Springer, Berlin, 1985.

 ^[2] J. Jortner, Femtochemistry, Ultrafast Chemical and Physical Processes in Molecular Systems,
 M. Chergui (ed.), World Scientific, Singapore, 1996, p. 15.

^[3] I.Ya. Fugol', Adv. Phys. 27 (1978) 1.

^[4] I.Ya. Fugol', Adv. Phys. 37 (1988) 1.

^[5] V.E. Bondybey, Adv. Chem. Phys. 41 (1980) 269.

^[6] M. Chergui, N. Schwentner, W. Böhmer, J. Chem. Phys. 85 (1986) 2472.

^[7] M. Chergui, N. Schwentner, V. Shandrasekharan, J. Chem. Phys. 89 (1988) 1277.

^[8] F. Vigliotti, M. Chergui, M. Dickgiesser, N. Schwentner, Faraday Discuss. 108 (1997) 139.

^[9] F. Vigliotti, M. Chergui, Chem. Phys. Lett. 296 (1998) 316.

^[10] F. Vigliotti, M. Chergui, Chem. Phys. Lett. 'Erratum' 305 (1999) 187.

^[11] M. Chergui, C. R. Acad. Sci. 2 (2001) 1453.

^[12] M.T. Portella-Orbeli, C. Jeannin, M. Chergui, Chem. Phys. Lett. 259 (1996) 475.

^[13] C. Jeannin, M.T. Portella-Orbeli, F. Vigliotti, M. Chergui, Chem. Phys. Lett. 279 (1997) 65.

^[14] C. Jeannin, M.T. Portella-Orbeli, S. Jiménez, F. Vigliotti, B. Lang, M. Chergui, Chem. Phys. Lett. 316 (2000) 51.

- [15] F. Vigliotti, L. Bonacina, M. Chergui, G. Rojas-Lorenzo, J. Rubayo-Soneira, Chem. Phys. Lett. 362 (2002) 31.
- [16] F. Vigliotti, L. Bonacina, M. Chergui, Phys. Rev. B 67 (2003) 115118.
- [17] M. Lengen, M. Joppien, R. von Pietrowski, T. Möller, Chem. Phys. Lett. 229 (1994) 362.
- [18] O. Bjorneholm, F. Federmann, F. Fösing, T. Möller, Phys. Rev. Lett. 74 (1995) 3017.
- [19] O. Bjorneholm, F. Federmann, F. Fösing, T. Möller, S. Stampfli, J. Chem. Phys. 104 (1996) 1876.
- [20] J. Wörmer, R. Karnbach, M. Joppien, T. Möller, J. Chem. Phys. 104 (1996) 8269.
- [21] D. Scharf, J. Jortner, U. Landman, J. Chem. Phys. 88 (1988) 4273.
- [22] A. Goldberg, A. Heidenreich, J. Jortner, J. Phys. Chem. 99 (1995) 2662.
- [23] A. Goldberg, J. Jortner, J. Chem. Phys. 107 (1997) 8994.
- [24] J. Goodman, L.E. Brus, J. Chem. Phys. 67 (1977) 933.
- [25] J. Goodman, L.E. Brus, J. Chem. Phys. 69 (1978) 4083.
- [26] S. Jiménez, A. Pasquarello, R. Car, M. Chergui, Chem. Phys. 233 (1998) 343.
- [27] S. Jiménez, M. Chergui, G. Rojas-Lorenzo, J. Rubayo-Soneira, J. Chem. Phys. 114 (2001) 5264.
- [28] G. Rojas-Lorenzo, J. Rubayo-Soneira, F. Vigliotti, M. Chergui, Phys. Rev. B 67 (2003) 115119.
- [29] J.C. Castro Palacios, L. Velázquez, G. Rojas-Lorenzo, J. Rubayo-Soneira, J. Mol. Struc. Theochem 730 (2005) 253.
- [30] U. Weiss, Quantum Dissipative Systems, World Scientific, Singapore, 1993, 3rd. ed.
- [31] H.-P. Breuer, F. Petruccione, The Theory of Open Quantum Systems, Clarendon, Oxford, 2006.
- [32] S. Miret-Artés, E. Pollak, J. Phys.: Condens. Matter 17 (2005) S4133.
- [33] R. Martínez-Casado, J.L. Vega, A.S. Sanz, S. Miret-Artés, Phys. Rev. Lett. 98 (2007) 216102.
- [34] R. Martínez-Casado, J.L. Vega, A.S. Sanz, S. Miret-Artés, Phys. Rev. E 75 (2007) 051128.
- [35] R. Martínez-Casado, J.L. Vega, A.S. Sanz, S. Miret-Artés, J. Phys.: Condens. Matter 19 (2007) 305002.
- [36] R. Martínez-Casado, J.L. Vega, A.S. Sanz, S. Miret-Artés, Phys. Rev. B 77 (2008) 115414.
- [37] A.O. Caldeira, A. J. Leggett, Ann. Phys. (N.Y.) 149 (1983) 374.
- [38] A.O. Caldeira, A. J. Leggett, Ann. Phys. (N.Y.) 153 (1984) 445.
- [39] V.B. Magalinskii, Sov. Phys. JETP 9 (1959) 1381.

- [40] E. Pollak, H. Grabert, P. Hänggi, J. Chem. Phys. 91 (1989) 4037.
- [41] P. Hänggi, P. Talkner, M. Borkovec, Rev. Mod. Phys. 62 (1990) 251.
- [42] R. Martínez-Casado, A.S. Sanz, S. Miret-Artés, J. Chem. Phys., submitted for publication. pre-print arXiv:0810.1826.
- [43] R. Martínez-Casado, G. Rojas-Lorenzo, J.L. Vega, A.S. Sanz, S. Miret-Artés, Chem. Phys., submitted for publication. pre-print: arXiv:0909.0719.
- [44] S.A. Adelman, M.W. Balk, J. Chem. Phys. 81 (1984) 5117.
- [45] S.A. Adelman, R.H. Stote, J. Chem. Phys. 88 (1988) 4397.
- [46] S.A. Adelman, R. Muralidhar, R.H. Stote, J. Chem. Phys. 99 (1993) 1333.
- [47] F. Vigliotti, E. Sarraf, M. Chergui, R. Scholz, Phys. Rev. Lett. 83 (1999) 2355.
- [48] J.P. Bergsma, P.H. Berens, K.R. Wilson, D.R. Fredkin, E.J. Heller, J. Phys. Chem. 88 (1984) 612.
- [49] M.P. Allen, D.J. Tildesley, Computer Simulation of Liquids, Clarendon, Oxford, 1987.